EBioMedicine 66 (2021) 103290

Contents lists available at ScienceDirect

EBioMedicine

journal homepage: www.elsevier.com/locate/ebiom

Research paper

Conjugated secondary 12α-hydroxylated bile acids promote liver fibrogenesis

Guoxiang Xie[a,b,†], Runqiu Jiang[c,†], Xiaoning Wang[d,†], Ping Liu[d], Aihua Zhao[a], Yiran Wu[e], Fengjie Huang[b], Zhipeng Liu[f], Cynthia Rajani[g], Xiaojiao Zheng[a], Jiannan Qiu[d], Xiaoling Zhang[h], Suwen Zhao[e], Hua Bian[i], Xin Gao[i], Beicheng Sun[c], Wei Jia[a,g,j,k,*]

[a] *Center for Translational Medicine, Shanghai Jiao Tong University Affiliated Sixth People's Hospital, Shanghai 200233, China*
[b] *Human Metabolomics Institute, Inc., Shenzhen, Guangdong 518109, China*
[c] *Department of Hepatobiliary Surgery, The Drum Tower Hospital Affiliated to Nanjing University Medical School, Nanjing, Jiangsu 210009, China*
[d] *E-institute of Shanghai Municipal Education Committee, Institute of Interdisciplinary Integrative Medicine Research, Shanghai University of Traditional Chinese Medicine, Shanghai 201203, China*
[e] *The iHuman Institute, ShanghaiTech University, Shanghai 201210, China*
[f] *Medical School of Southeast University, Nanjing, Jiangsu 210096, China*
[g] *University of Hawaii Cancer Center, Honolulu, HI 96813, USA*
[h] *Department of Hygienic Analysis and Detection, Nanjing Medical University, Nanjing, Jiangsu 211166, China*
[i] *Department of Endocrinology and Metabolism, Zhongshan Hospital, Fudan University, Shanghai 200032, China*
[j] *Hong Kong Traditional Chinese Medicine Phenome Research Centre, School of Chinese Medicine, Hong Kong Baptist University, Kowloon Tong, Hong Kong 999077, China*
[k] *Lead contact*

ARTICLE INFO

Article History:
Received 27 September 2020
Revised 24 February 2021
Accepted 4 March 2021
Available online xxx

Keywords:
Liver fibrosis
Hepatic stellate cell
12α-hydroxylated bile acids
G protein-coupled bile acid receptor
TGR5
p38MAPK
ERK1/2

ABSTRACT

Background: Significantly elevated serum and hepatic bile acid (BA) concentrations have been known to occur in patients with liver fibrosis. However, the roles of different BA species in liver fibrogenesis are not fully understood.

Methods: We quantitatively measured blood BA concentrations in nonalcoholic steatohepatitis (NASH) patients with liver fibrosis and healthy controls. We characterized BA composition in three mouse models induced by carbon tetrachloride (CCl_4), streptozotocin-high fat diet (STZ-HFD), and long term HFD, respectively. The molecular mechanisms underlying the fibrosis-promoting effects of BAs were investigated in cell line models, a 3D co-culture system, and a Tgr5 (HSC-specific) KO mouse model.

Findings: We found that a group of conjugated 12α-hydroxylated (12α-OH) BAs, such as taurodeoxycholate (TDCA) and glycodeoxycholate (GDCA), significantly increased in NASH patients and liver fibrosis mouse models. 12α-OH BAs significantly increased HSC proliferation and protein expression of fibrosis-related markers. Administration of TDCA and GDCA directly activated HSCs and promoted liver fibrogenesis in mouse models. Blockade of BA binding to TGR5 or inhibition of ERK1/2 and p38 MAPK signaling both significantly attenuated the BA-induced fibrogenesis. Liver fibrosis was attenuated in mice with Tgr5 depletion.

Interpretation: Increased hepatic concentrations of conjugated 12α-OH BAs significantly contributed to liver fibrosis via TGR5 mediated p38MAPK and ERK1/2 signaling. Strategies to antagonize TGR5 or inhibit ERK1/2 and p38 MAPK signaling may effectively prevent or reverse liver fibrosis.

Fundings: This study was supported by the National Institutes of Health/National Cancer Institute Grant 1U01CA188387-01A1, the National Key Research and Development Program of China (2017YFC0906800); the State Key Program of National Natural Science Foundation (81430062); the National Natural Science Foundation of China (81974073, 81774196), China Postdoctoral Science Foundation funded project, China (2016T90381), and E-institutes of Shanghai Municipal Education Commission, China (E03008).

* Corresponding author.
E-mail address: weijia1@hkbu.edu.hk (W. Jia).
† These authors contributed equally to this work.

https://doi.org/10.1016/j.ebiom.2021.103290

Research in context

Evidence before this study

BAs are synthesized in the liver via two different routes, the classical or neutral pathway, producing BAs that had undergone hydroxylation at the carbon 12 position (12α-OH BAs), and the alternative (or acidic) pathway to produce non-12α-OH BAs. Significantly elevated serum and hepatic BA concentrations have been known to occur in patients with liver fibrosis. However, the roles of different BA species in liver fibrogenesis are not fully understood.

Added value of this study

We found that the levels of BAs (especially 12α-OH BAs) were significantly increased in human serum and mouse plasma, and in mouse liver. Conjugated secondary 12α-OH BAs, TDCA and GDCA, most effectively upregulated hepatic stellate cells (HSC) proliferation and protein expression of fibrosis-related markers, including α-SMA, TGF-ß, COL I, and PDGF via strong binding affinity to TGR5, and sustained activation of downstream ERK1/2 and p38 MAPK. Administration of TDCA and GDCA directly activated HSCs and promoted liver fibrogenesis in a CCl_4-induced liver fibrosis C57BL/6J mouse model. Reduction of p38 MAPK and ERK 1/2 phosphorylation or inhibition of TGR5 expression can significantly reduce proliferation and activation of HSC using a CCl_4-induced liver fibrosis Rosa26-LSL-Cas9 knockin mouse model with depleted Tgr5 in HSCs.

Implications of all the available evidence

Increased hepatic concentrations of conjugated 12α-OH BAs significantly contributed to liver fibrosis. Strategies to increase the hepatic BA clearance or to block BA binding to TGR5 in HSCs using TGR5 antagonists may be effective for liver fibrosis prevention and treatment.

Introduction

Liver fibrosis is caused by dysregulated wound healing from chronic liver injuries. Approximately 15−20% of patients with fatty liver progress to fibrosis and cirrhosis [1,2] and about 15−50% of non-alcoholic steatohepatitis (NASH) patients develop severe fibrosis [3,4]. In the liver, ongoing fibrogenesis ultimately leads to cirrhosis. Recent studies showed that liver fibrosis could be reversed in a variety of liver diseases [5,6]. However, the vast majority of patients with liver fibrosis do not achieve remission or regression after the cessation of the cause of liver injury, suggesting that some important factors that contribute to liver fibrogenesis have yet to be identified.

A common metabolic phenotype as characterized by significantly increased serum and hepatic bile acids (BAs) has been widely reported in patients with chronic liver disease [7]. BAs are synthesized from cholesterol in the liver by several enzymes. There are two major pathways, the classical (or neutral) pathway and the alternative (or acidic) pathway in BA synthesis [8]. Classical pathway is initiated by CYP7A1, which is the rate-limiting enzyme, to convert cholesterol to cholic acid (CA) and chenodeoxycholic acid (CDCA). CYP8B1 enzyme is required for CA synthesis in classical pathway. The alternative pathway is initiated by CYP27A1 and followed by CYP7B1 to generate CDCA [9]. The structural difference between CA and CDCA is that CA and its derivatives has a 12α-OH that catalyzed by CYP8B1, while CDCA and its derivatives were non-12α-OH BAs without 12-hydroxylation. In general, BAs are synthesized in the liver via two different routes, the classical or neutral pathway, producing BAs that had undergone hydroxylation at the carbon 12 position (12α-OH BAs, i.e., cholic acid (CA), deoxycholic acid (DCA), and their taurine- and glycine-conjugated derivatives), and the alternative (or acidic) pathway to produce non-12α-OH BAs (chenodeoxycholic acid (CDCA), lithocholic acid (LCA), and ursodeoxycholic acid (UDCA), and their taurine- and glycine-conjugated derivatives). As important signaling molecules, BAs play a critical role in the regulation of hepatic metabolic homeostasis by activating or inhibiting nuclear farnesoid X receptor (FXR) and membrane G-protein-coupled receptor (TGR5) [10,11]. TGR5 is expressed in Kuppfer cells as well as activated hepatic stellate cells (HSCs) [12], and mediates BA-induced HSC activation [13].

Of the two pathways of hepatic BA synthesis, the alternative pathway is increasingly recognized to play a key role in the regulation of lipid, cholesterol, carbohydrate, and energy homeostasis [14]. Additionally, increased ratio of 12α-OH BAs resulting from dysregulation of the alternative pathway leads to a loss in its ability to control lipid homeostasis and inflammatory conditions [14,15]. Increased 12α-OH BA levels have been identified in human diabetic patients [16] and NASH patients [17]. Our recent studies also demonstrated that increased 12α-OH BA levels were associated with unhealthy high BMI status [18] and that the activation of the alternative BA synthetic pathway effectively lowered blood and hepatic lipid levels in mouse models [19]. In this work, we investigated the mechanistic role of BAs in liver fibrogenesis in which 12α-OH BAs strongly bound to TGR5 and sustained activation of downstream ERK1/2 and p38 MAPK, leading to significantly increased HSC proliferation and protein expression of fibrosis-related markers. Liver fibrosis can be reversed by Tgr5 depletion or inhibition of ERK1/2 and p38 MAPK signaling.

Materials and methods

Clinical studies

Liver fibrosis patients and healthy controls

Fasting serum samples were collected from NASH patients with liver fibrosis (n = 99) recruited from Zhongshan Hospital, Fudan University and healthy controls (n = 99) recruited from Shuguang Hospital Affiliated to Shanghai University of Traditional Chinese Medicine, Shanghai, China. Liver specimens were obtained from all patients to confirm liver fibrosis.

Biopsy liver tissues from 15 NASH patients with higher 12α-OH BA levels ($>$ 5 μg/mL) and 15 age and sex matched NASH patients with lower 12α-OH BA levels ($<$ 1 μg/mL) were subject to immunofluorescence staining. Normal liver tissues were obtained from 15 patients who had non-fibrotic and non-tumor diseases such as liver hemangioma and hepatic calculi (The First Affiliated Hospital of Nanjing Medical University, Nanjing, China).

The samples were provided in de-identified fashion and the lab staffs were blinded to the clinical information. The study was approved by the institutional human subjects review board of the hospitals (approval no. 2012-206-22-01, B2013-132). All participants signed informed consent for the study.

Serum sample collection and analysis

Overnight fasting blood samples were collected from all subjects and centrifuged at 3000 $\times$ g for 10 min at room temperature. The resulting sera were aliquoted and stored at −80 °C until analysis. Hematological (COULTER LH750 Hematology Analyzer, USA) or common biochemical tests (Beckman Coulter Synchron DXC800, USA) were performed using standard methodologies. The coagulation function was evaluated using an automatic coagulation analyzer (STAGO Compact, Diagnostica Stago, France).

Animal study

Experimental 1. Long term HFD-fed mice model. We fed C57BL/6J male mice with HFD alone to observe the liver fibrogenesis. Two groups of mice were included: (1) control, mice were fed chow diets consisting of 10% fat, 71% carbohydrate, and 19% protein; (2) HFD, mice were fed with diets consisting of 45% fat, 36% carbohydrate, and 19% protein. We sacrificed mice at week 82, we observed fibrosis formation in HFD-fed mice. Blood serum and liver samples were collected at week 82 for BA assessment. All samples were stored at -80° C until analysis. The animal experiments were performed with approval of the Institutional Animal Care and Use Committee from Shanghai Jiao Tong University Affiliated Sixth People's Hospital.

Experimental 2. STZ-HFD-induced NASH-HCC C57BL/6J mouse model

New born male C57BL/6J mice (Vital River Laboratory Animal Technology Co. Ltd., Beijing, China) were randomly divided into two groups: (1) control mice were housed without any treatment and fed normal chow (12% calorie from fat), and (2) NASH-HCC mice received a single subcutaneous injection of 200 μg STZ (Sigma, MO, USA) 2 days after birth and were fed with HFD (60% calorie from fat) *ad libitum* at 4 weeks of age for 8 weeks[37]. Body weight was measured weekly. At week 12, 8 mice in each group were euthanized and their livers were removed and stored at −80°C for analyses. Plasma and liver samples were collected for biochemical, histological and BA quantitation.

The animal experiments were performed with approval of the Institutional Animal Care and Use Committee from Shanghai University of Traditional Chinese Medicine.

Experimental 3. Carbon tetrachloride (CCl_4)-induced liver fibrosis C57BL/6J mouse model

CCl_4-induced liver fibrosis mouse model was also developed to investigate the role of GDCA and TDCA in liver fibrogenesis. C57BL/6J mice (8 weeks old) was divided into 4 groups (n = 8 in each group): (1) corn oil group, ip with corn oil as vehicle; (2) CCl_4 group, ip with 0.5 g/kg body weight CCl_4 in corn oil (equivalent to 200 μL/mouse) 3 times a week for 5 weeks; (3) CCl_4+TDCA+GDCA group, ip with 0.5 g/kg body weight CCl_4 in corn oil (equivalent to 200 μL/mouse) and TDCA and GDCA (at the dose of 500 mg/kg, respectively) using a plastic feeding tube 3 times a week for 5 weeks; (4) TDCA+GDCA group, the mice were fed with TDCA and GDCA (at the dose of 500 mg/kg, respectively) using a plastic feeding tube 3 times a week for 5 weeks. Twenty-four hours after the last challenge, all mice were sacrificed. All procedures were performed under sterile conditions.

The animal experiments were performed with approval of the Institutional Animal Care and Use Committee from Shanghai University of Traditional Chinese Medicine.

Experimental 4. CCl_4-induced liver fibrosis Rosa26-LSL-Cas9 knock in mouse model

CCl_4-induced liver fibrosis mouse model was also developed to investigate the role of TGR5 in liver fibrogenesis. Rosa26-LSL-Cas9 knockin mice (CAS9 KI, 8 weeks old) purchased from Jackson lab (https://www.jax.org/strain/024857) was divided into 4 groups (n = 8 in each group): (1) CAS9 KI+ corn oil group, ip with corn oil as vehicle; (2) CAS9 KI+CCl_4 group, ip with 0.5 g/kg body weight CCl_4 in corn oil (equivalent to 200 μL/mouse) 2 times a week for 5 weeks; (3) CAS9 KI+ CCl_4+Tgr5 sgRNA group, the mice were treated with 100 μL adeno-associated virus (AAV) containing Gfap-Cre-U6-Tgr5 sgRNA cassette (virus concentration: 5.5E+10/mL) via intrasplenic injection once a week and ip with 0.5g/kg body weight CCl_4 in corn oil (equivalent to 200 μL/mouse) 2 times a week for 5 weeks. The AAV can deplete Tgr5 expression specifically in HSCs due to the Gfap- promoter-driving- Cre recombinase expression. Twenty-four hours after the last challenge, all mice were sacrificed. All procedures were performed under sterile conditions. Serum and liver samples were collected for biochemical, histological and BA quantitation.

Animal welfare and the animal experimental protocols were strictly consistent with the Guide for the Care and Use of Laboratory Animals (U.S. National Research Council, 1996) and the related ethics regulations of Nanjing University Medical School.

Liver biochemistry

Alanine aminotransferase (ALT) and aspartate aminotransferase (AST) levels were assessed using commercially available kits (Ke Hua, Shanghai, China), according to manufacturer's instructions.

HSCs isolation and culture

Primary mouse HSCs were isolated from livers of CAS9 KI mice according to a modified method previously described [20]. The isolated cells were plated on uncoated plastic 10 cm-diameter plate at a density of 5×10^6. After the first 24 h, nonadherent cells and debris were removed. Cell viability was greater than 90%, as assessed by trypan blue exclusion. Purity was 90−95%, as assessed by a typical light microscopic. Then, the cells were trypsinized and plated on a 6-well plate at 5×10^5 per well. Isolated HSCs were treated with 50 μL adeno-associated virus (AAV) (virus concentration: 5.5E+8/mL) or control for 24 h, and further treated with 12α-OH BA2 and vehicle control (50 μM) for 48 h.

Cell culture studies

2D. cell culture

Human hepatic stellate cell line LX-2 was purchased from EMD Millipore and hepatocyte cell line L02 was purchased from the Shanghai Institute of Cell Biology of the Chinese Academy of Science, China. Both cell lines were maintained in Dulbecco's modified Eagle's medium (Invitrogen) supplemented with 10% fetal bovine serum (FBS, Gibco, USA). All cell lines tested negative for mycoplasma contamination.

3D. co-culture system

A 3D culture system were setup by mixing HSCs (LX-2) with L02 at a ratio of 1:100 in a 3D Petri Dish® (Micro-Tissues) (RI, USA), which was a scaffold-free culture system maximizing cell-to-cell interactions.

Cell culture treatments

Individual BAs were obtained from Sigma-Aldrich (St. Louis, MO, USA), Steraloids Inc. (Newport, RI, USA) and TRC Chemicals (Toronto, ON, Canada). Cells were treated with individual BAs at 25, 50, 75, and 100 μM for 24 hours. A combination of equal amounts of TCA and GCA (50 μM each, termed as 12α-OH BA1), or a combination of equal amount of TDCA and GDCA (50 μM each, termed as 12α-OH BA2) for varied lengths of time as specified in the Results section. Cells treated with DMSO were used as a vehicle control. SCH772984 (S7101, ERK1/2 inhibitor), SP600125 (S1460, JNK inhibitor),SB239063 (S7741, p38MAPK inhibitor), SQ22536 (s8283, inhibitor for adenylyl cyclase (AC)) and KG-501 (s8409, inhibitor for CREB) were purchased from Selleck Chemicals. TGR5 antagonist 5β-cholanic acid (C7628) was purchased from Sigma-Aldrich. The siRNA targeting human TGR5 (sc-61678-SH) and control shRNA plasmid (sc-108060) were purchased from Stanta Cruz (Dallas, TX).

ELISA for cAMP measurement

The cell lines were plated into 24 well-plates with an initial cell density of 2×10^5 cells/well, and treated with BAs at 25 μM for 1 h. The intracellular cAMP was extracted, and determined using a cAMP

Assay Kit according to the manufacturer's instruction (ab138880, Abcam).

Cell proliferation assays

Number of liver cells was determined using a WST-8-based Cell Counting Kit 8 (CCK-8) (Dojin Laboratories, Kumamoto, Japan) according to the manufacturer's instructions. Briefly, the cells were seeded at a density of 1×10^3 cells/well in 96-well plates. CCK-8 solution (10 μL) was added to each well containing 100 μL of the culture medium, and the plate was incubated for 2 h at 37 °C. Viability of cells were evaluated by measuring the absorbance at 450 nm using a microplate reader (Molecular Devices, Menlo Park, CA).

RNA isolation and quantitative reverse transcription PCR (qRT-PCR)

Total RNA was isolated with Trizol (Thermo Fisher Scientific, CA) according to the manufacturer's instruction. cDNA was synthesized from the total RNA using iScript Reverse Transcription Supermix for RT-qPCR (Bio-Rad CA). Transcript levels were measured in duplicate by qRT-PCR (LightCycler 480 II, Roche) using iTaq™ Universal SYBR® Green Supermix (Bio-Rad CA). Expression levels were normalized to house-keeping gene GAPDH. Primer sequences are listed in Table S6.

Western blot

The whole cell lysates were prepared as previously described [21]. Boiled samples containing equal amount of total protein were loaded on 10% SDS-PAGE gels for electrophoresis separation, and transferred onto PVDF membranes for antigen detection. The signal was visualized using an ECL kit (Bio-rad, CA). Antibodies for p-ERK1/2 (4370), p-p38 MAPK (4511), p-JNK (4668), ERK1/2 (4695), p38 MAPK (8690) and JNK (9252) were purchased from Cell signaling Technology (Danvers, MA); and antibodies for TGR5 (ab32027), α-SMA (ab7817), COL I (ab21286), TGF-β (ab92486), β-actin (ab6276) were purchased from Abcam (Cambridge, MA).

Sirius red, immunohistochemistry and immunofluorescence staining

Liver fibrosis status of the mice was evaluated using a Picro Sirius Red Stain Kit (ab150681). Paraffin-embedded and formalin-fixed mouse liver samples were used for immunohistochemistry staining as previously described [22], and antibodies used in this procedure including α-SMA (ab7817), TGF-β (ab92486), COL I (ab21286), and PDGF (ab51869), were purchased from Abcam (Cambridge, MA). For immunofluorescence analysis, tissue slides were stained with antibodies including α-SMA (ab7817), TGF-β (ab92486), TGR5(ab32027), p-ERK1/2 (4370) and p-p38 MAPK (4511) purchased from Abcam (Cambridge, MA), followed by staining with Alexa Fluor 488-conjugated anti-mouse IgG (1:500, Ab150117), goat anti-rabbit IgG (H+L) superclonal secondary antibody conjugated with Biotin (A27035), and Streptavidin (PE-Cy5.5) (SA1018) (Thermo Fisher Scientific, CA). Stain-positive cells were quantified using Image J software (NIH).

Binding affinity analysis

The BA-TGR5 binding affinity analysis was performed using the Schrodinger Suite 2015-4 (Schrödinger, LLC, NY). Homology model was built based on crystal structure of the active state adenosine A_{2A} receptor (PDBID: 5G53) [23] using the Advanced Homology Modeling tool (Prime, version 4.2, Schrödinger, LLC, New York, NY, 2015). 2D to 3D structure conversion of ligand binding was performed using the LigPrep software (LigPrep, version 3.6, Schrödinger, LLC, New York, NY, 2015). Molecular docking was analyzed using the Induced Fit Docking tool (Induced Fit Docking protocol 2015-4, Glide version 6.4, Prime version 3.7. 2015, Schrödinger, LLC, New York, NY, 2015).

Quantification of BAs

Concentrations of BAs in serum/plasma and liver were measured according to previously reported methods [24]. Briefly, extracts of serum, plasma and liver along with BA reference standards were analyzed using a Waters ACQUITY ultra performance LC system coupled with a Waters XEVO TQ-S mass spectrometer with an ESI source controlled by MassLynx 4.1 software (Waters, Milford, MA). Chromatographic separations were performed using an ACQUITY BEH C18 column (1.7 μm, 100 mm × 2.1 mm internal dimensions) (Waters, Milford, MA). UPLC-MS raw data obtained with negative mode were analyzed using the TargetLynx applications manager version 4.1 (Waters Corp., Milford, MA) to obtain calibration equations and the quantitative concentration of each BA in the samples. The levels of 12α-OH BAs were the sum of the concentration of CA, DCA, TCA, GCA, TDCA and GDCA in each samples, the levels of non-12α-OH BAs were the sum of the concentration of CDCA, LCA, UDCA, TCDCA, GCDCA, TLCA, GLCA, TUDCA and GUDCA in each sample. The levels of total BAs were the sum of all the BAs quantified in the samples.

Metagenomic analysis

Total microbial genomic DNA samples were extracted using the DNeasy PowerSoil Kit (QIAGEN, Inc., Netherlands), according to the manufacturer's instructions, and stored at -20 °C prior to further assessment. The quantity and quality of extracted DNAs were measured using a NanoDrop ND-1000 spectrophotometer (Thermo Fisher Scientific, Waltham, MA, USA) and agarose gel electrophoresis, respectively. The extracted microbial DNA was processed to construct metagenome shotgun sequencing libraries with insert sizes of 400 bp by using Illumina TruSeq Nano DNA LT Library Preparation Kit. Each library was sequenced by Illumina HiSeq X-ten platform (Illumina, USA) with PE150 strategy at Personal Biotechnology Co., Ltd. (Shanghai, China).

Raw sequencing reads were processed to obtain quality-filtered reads for further analysis. The sequencing adapters were removed from sequencing reads using Cutadapt (v1.2.1). Low quality reads were trimmed using a sliding-window algorithm. The sequencing reads were aligned to the host genome using BWA (http://bio-bwa.sourceforge.net/) to remove host contamination. The quality-filtered reads were de novo assembled to construct the metagenome for each sample by IDBA-UD (Iterative De Bruijn graph Assembler for sequencing data with highly Uneven Depth). All coding regions (CDS) of metagenomic scaffolds longer than 300 bp were predicted by MetaGeneMark. CDS sequences of all samples were clustered by CD-HIT at 90% protein sequence identity, to obtain non-redundant gene catalog. Gene abundance in each sample was estimated by soap coverage based on the number of aligned reads. The lowest common ancestor taxonomy of the non-redundant genes was obtained by aligning them against the NCBI-NT database by BLASTN (e value < 0.001). The functional profiles of the non-redundant genes were obtained by annotated against the GO, KEGG, EggNOG and CAZy databases, respectively, by using DIAMOND alignment algorithm.

Statistical analysis

The differences between groups in BA concentrations were analyzed using t-tests and the Holm-Sidak multiple comparisons correction in Graphpad Prism 6.0 (GraphPad Software, CA, USA). We considered $p < 0.05$ as statistically significant.

Results

Liver fibrosis in NASH patients was associated with significantly increased serum concentrations of 12α-OH BAs

We quantitatively profiled BAs in the sera of NASH patients with fibrosis (n = 99) and matched healthy controls (n = 99). The

demographic and clinical characteristics of the two groups are detailed in Table S1. The BA concentrations were found significantly higher in the sera of NASH patients with liver fibrosis than in controls (Fig. 1A, Table S2). Notably, the concentration of 12α-OH BAs was higher than non-12α-OH BAs in NASH patients (Fig. 1B) as well as in HBV and HCV patients with fibrosis (Fig. S1) and the average fold change (FC) (patients *vs.* controls) of 12α-OH BAs was much greater than those of non-12α-OH BAs (Fig. 1C). Moreover, patients with high 12α-OH BAs (>5 μg/mL, n = 15) in serum also had greater α-smooth muscle actin (α-SMA, a fibrosis marker) protein expression in the liver relative to those with low 12α-OH BAs (<1 μg/mL, n = 15) in serum (Fig. 1D). Masson trichrome staining showed significant higher level of fibrosis score in patients with high 12α-OH BAs than in those with low 12α-OH BAs in serum (Fig. 1E).

Liver fibrosis was associated with significantly increased hepatic 12α-OH BA levels in three mouse models

First, liver fibrosis was developed in the mice fed with high fat diet (HFD) for 82 weeks, as shown by histological changes in the liver (H&E staining) (Fig. 2A). Compared with control mice, the HFD-treated mice had greater fibrosis level (Sirius red staining, α-SMA protein expression, and gene expression on α-SMA and collagen I (COL I)) (Fig. 2A and Fig. S2). In addition, the liver-to-body weight ratio of the HFD-treated mice was 1.61-fold higher (p = 0.0000035) than that of the control mice (Fig. S3A); and compared with the controls (Fig. S3B), serum alanine aminotransferase (ALT) and aspartate aminotransferase (AST) levels also increased by FC = 2.26 (p = 0.0032) and FC= 1.74 (p = 0.00019), respectively, in the fibrotic mice. Notably, similar to the BA profile in NASH

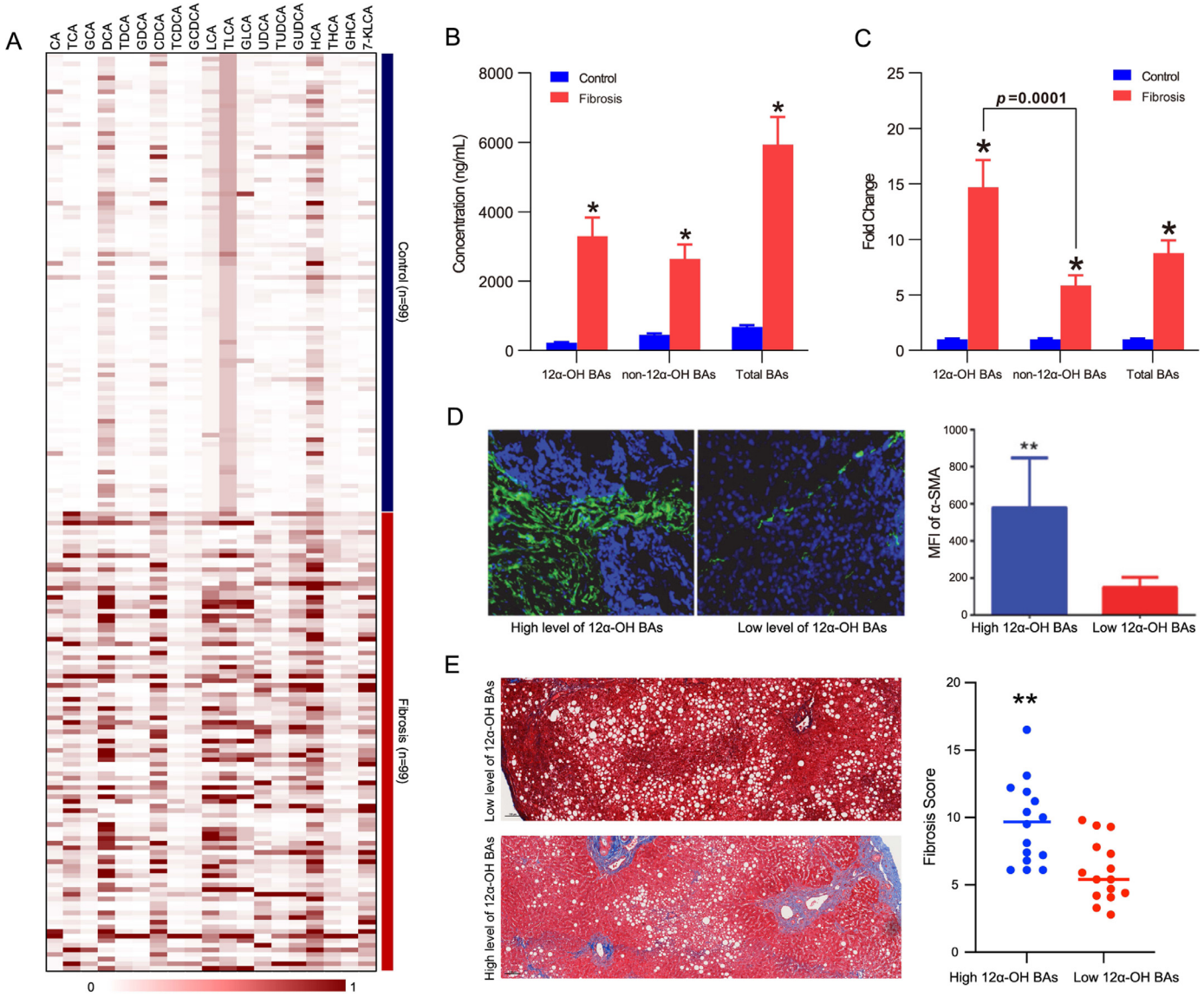

Fig. 1. The BA concentrations were significantly higher in the sera of NASH patients with liver fibrosis (n = 99) than in the controls (n = 99). (A) Heatmap of serum BA concentrations (scaled to 0-1) in NASH patients and controls. Red and white represent high and low BA concentration, respectively (see color scale). **(B)** Concentration of 12α-OH BAs, non-12α-OH BAs, and total BAs that were higher in NASH patients with fibrosis than in the controls. **(C)** Changes of 12α-OH BAs, non-12α-OH BAs, and total BAs in NASH patients with fibrosis vs. controls. **(D)** Immunofluorescence staining showed that α-SMA levels were significantly higher in the liver of fibrosis patients who had higher serum 12α-OH BAs (> 5 μg/mL, n = 15) than in those with lower serum 12α-OH BAs (< 1 μg/mL, n = 15). *p<0.05, compared to controls. (E) Masson trichrome staining showed significant higher level of fibrosis score in patients with high 12α-OH BAs than in those with low 12α-OH BAs in serum.

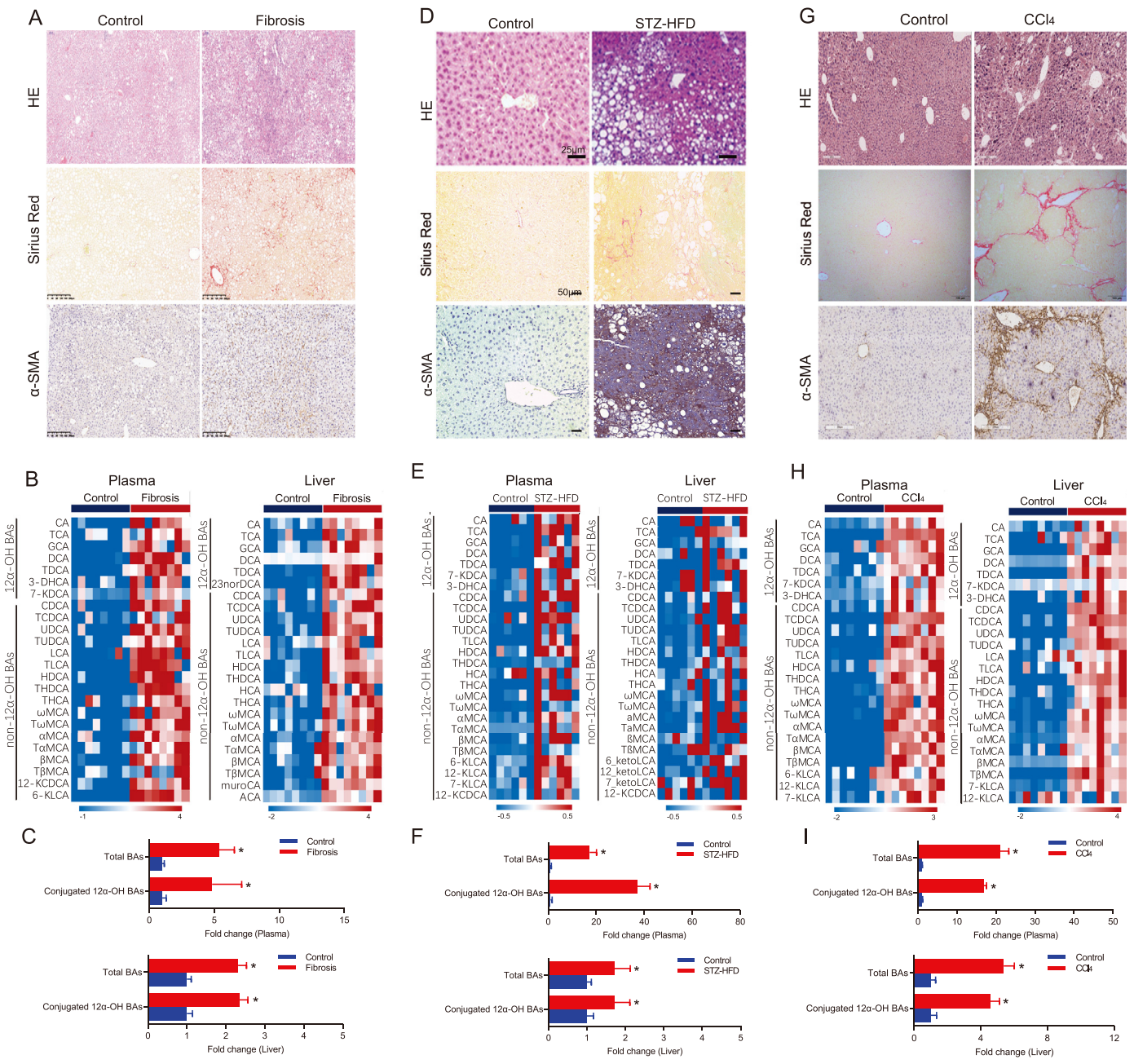

Fig. 2. Mice with liver fibrosis had higher concentrations of BAs in plasma and liver than control mice. **(A)** H&E, Sirius red staining and immunochemistry staining for α-SMA in stained liver sections from control and long term HFD-treated mice at week 82. Original magnifications X 200. **(B,C)** BAs levels in both plasma and liver were markedly increased in long term HFD-treated mice than in control mice. **(D)** H&E, Sirius red staining and immunochemistry staining for α-SMA in stained liver sections from control and STZ-HFD-treated mice at week 12. Original magnifications X 200. **(E,F)** BAs levels in both plasma and liver were markedly increased in STZ-HFD-treated mice than in control mice. **(G)** H&E, Sirius red staining and immunochemistry staining for α-SMA in stained liver sections from control and CCl_4-treated mice. Original magnifications X 200. **(H,I)** BAs levels in both plasma and liver were markedly increased in CCl_4-treated mice than in control mice.

patients, total BAs and 12α-OH BAs in liver and plasma were markedly increased in HFD-fed mice with fibrosis as compared to controls (Figs. 2B and 2C, Table S3).

Consistent with our previous publication [25], liver fibrosis was developed in the streptozotocin (STZ)-HFD treated mice, as shown by histological changes in the liver (H&E staining) (Fig. 2D). Compared with control mice, the STZ-HFD-treated mice had greater fibrosis level (Sirius red staining and α-SMA protein expression) in the liver (Fig. 2D). In addition, the liver-to-body weight ratio of the STZ-HFD-treated mice was 1.98-fold higher (p = 0.0007) than that of the control mice (Fig. S4A); and serum ALT and AST levels also increased by FC = 2.5 (p = 0.016) and FC = 1.9 (p = 0.025), respectively, in the STZ-HFD mice compared with the controls (Fig. S4B). The concentrations of 12α-OH and non 12α-OH BAs in the plasma and liver were significantly higher in the STZ-HFD-treated mice than in the controls (Fig. 2E, Table S4). Consistent with the human data, 12α-OH BAs significantly increased in both plasma and liver of the STZ-HFD mice compared to the controls (Fig. 2F, Table S4).

In the third fibrosis mouse model induced by carbon tetrachloride (CCl_4)-treatment (Fig. 2G), we found that liver fibrosis was associated with significantly increased total BAs and 12α-OH BAs in plasma and liver (Fig. 2H, I, Table S5). In addition, the liver-to-body weight ratio of the CCl_4-treated mice was 1.98-fold higher (p = 0.00012) than that of the control mice (Fig. S5A); and serum ALT and AST levels also

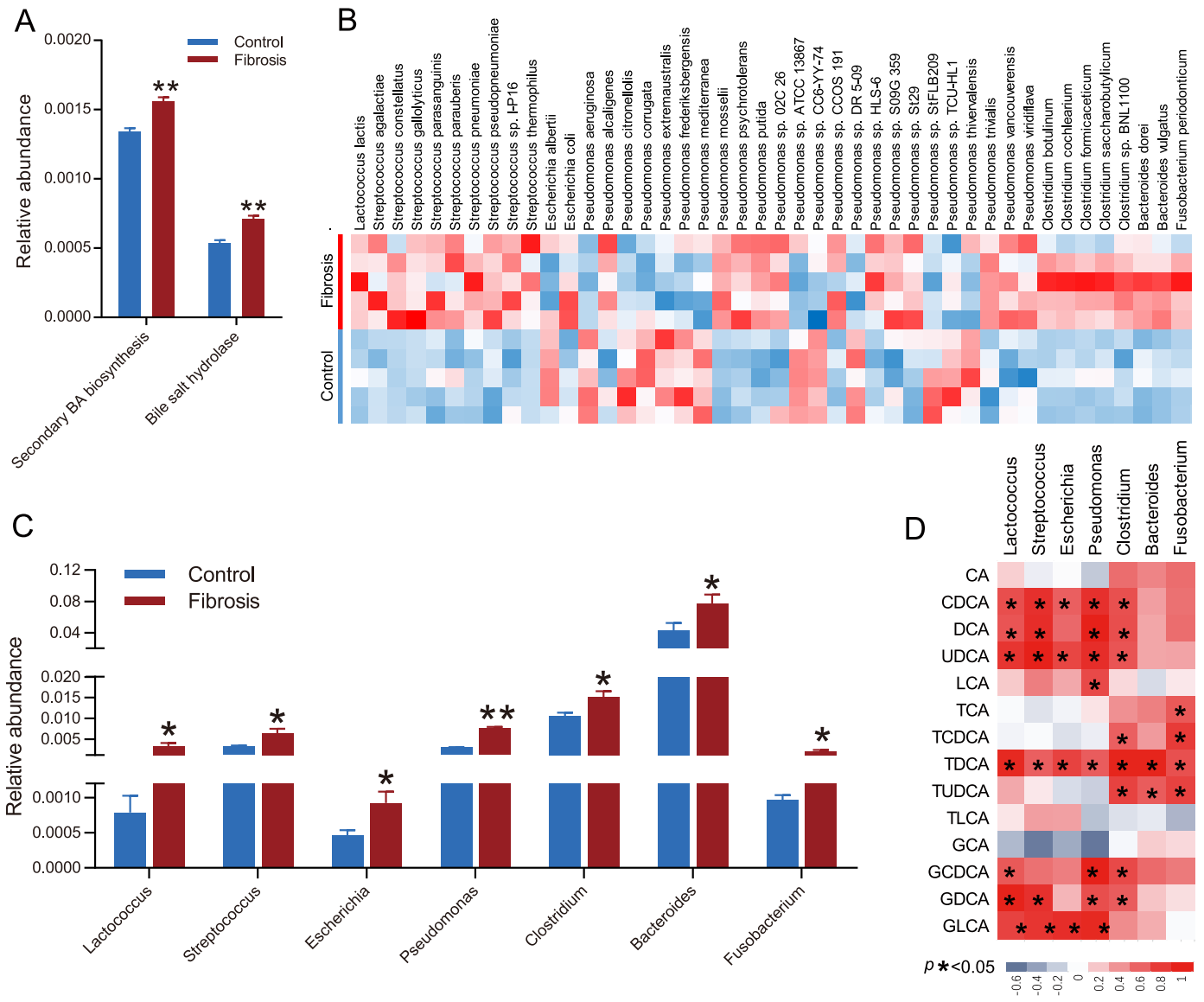

Fig. 3. **(A)** Function of secondary BA biosynthesis and bile salt hydrolase were significantly increased in mice with liver fibrosis. **(B)** Abundance of BA metabolism related microbiota at the genus level in ileum of fibrosis mice. **(C)** Abundance of BA metabolism related microbiota at the species level in ileum of fibrosis mice. **(D)** Spearman correlation between BA concentration and OTUs of BA metabolism-related microbes in mice with liver fibrosis. The color of each spot in the heatmap corresponds to the R value of the spearman correlation analysis between microbial abundance and BAs concentration, and the spot with * in red color spot refers to the significant positive correlation with R>0.3 and P<0.05 while the spot with * in blue color spot refers to the significant negative correlation with R<-0.3 and P<0.05.

increased by FC = 1.97 (p = 0.0040) and FC = 1.60 (p = 0.0027), respectively, in the CCl_4-treated mice compared with the controls (Fig. S5B).

Gut microbiota was significantly altered and correlated with altered BAs in mice with liver fibrosis

Our previous fecal microbiota analysis showed that the bacteria involved in the BA deconjugation, dehydroxylation, and BA degradation, such as *Clostridium* and *Bacteroides*, was altered significantly in mice with STZ-HFD treatment [25,26]. Gut microbiota analysis on CCl_4-treated mice also showed that gut microbiota alterations are associated with the development of an inflammatory environment, fibrosis progression and bacterial translocation [27]. Numbers of *Clostridium leptum* group and *Clostridium coccoides* group were significantly reduced in treated animals compared with control mice.

Our previous study on the role of HFD-induced BA changes in shaping the gut microbial composition in male C57BL/6 mice showed that HFD changes the relative composition of gut microbiota by increasing Firmicutes and decreasing Bacteroidetes at phylum levels along with alterations of the microbes at species levels [28]. HFD also remodeled the gut microbiota, characterized by increased *Bacteroides* and *Lactobacillus* genus [29], which can generate bile salt hydrolase (BSH). We here further conducted metagenomic analysis of microbiota in feces of long-term HFD treated mice with liver fibrosis. The analysis of KEGG function showed that function of secondary BA biosynthesis and BSH were significantly increased in mice with liver fibrosis (Fig. 3A). We also confirmed that the genus and species level of *Clostridium, Bacteroides, Lactococcus, Streptoccoccus, Escherichia, Pseudomonas*, and *Fusobacterium* were significantly increased (Fig. 3B and 3C) and were significantly positively correlated with fecal BAs including 12α-OH BAs (DCA, TDCA, GDCA, and TCA) and non-12α-OH BAs (CDCA, UDCA, LCA, TCDCA, TUDCA, GCDCA, and GLCA) concentrations in mice with liver fibrosis (Figs. 3D, S6). In detail, spearman correlation analysis between the gut microbiota changes and BA concentrations in feces in Fig. 3D showed that TDCA was significantly positively correlated with *Lactococcus* (r = 0.87, p = 0.002),

Streptococcus (r = 0.66, p = 0.044), *Escherichia* (r = 0.76, p = 0.012), *Pseudomonas* (r = 0.67, p = 0.039), *Clostridium* (r = 0.89, p = 0.001), *Bacteroides* (r = 0.89, p = 0.001), and *Fusobacterium* (r = 0.71, p = 0.027). There was also a significant positive correlation between GDCA was significantly positively correlated with *Lactococcus* (r = 0.90, p = 0.0008), *Streptococcus* (r = 0.82, p = 0.006), *Pseudomonas* (r = 0.72, p = 0.023), *Clostridium* (r = 0.67, p = 0.039). CDCA was significantly positively correlated with *Lactococcus* (r = 0.72, p = 0.023), *Streptococcus* (r = 0.82, p = 0.006), *Escherichia* (r = 0.66, p = 0.044), *Pseudomonas* (r = 0.82, p = 0.006), *Clostridium* (r = 0.71, p = 0.027). DCA was significantly positively correlated with *Lactococcus* (r = 0.70, p = 0.031), *Streptococcus* (r = 0.83, p = 0.005), *Pseudomonas* (r = 0.92, p = 0.0005), *Clostridium* (r = 072, p = 0.023). UDCA was significantly positively correlated with *Lactococcus* (r = 0.81, p = 0.007), *Streptococcus* (r = 0.92, p = 0.0005), *Escherichia* (r = 0.75, p = 0.017), *Pseudomonas* (r = 0.83, p = 0.005), *Clostridium* (r = 0.70, p = 0.031). LCA was significantly positively correlated with *Pseudomonas* (r = 0.73, p = 0.020). TCA was significantly positively correlated with *Fusobacterium* (r = 0.68, p = 0.035). TCDCA was significantly positively correlated with *Clostridium* (r = 0.66, p = 0.044), and *Fusobacterium* (r = 0.78, p = 0.011). TUDCA was significantly positively correlated with *Clostridium* (r = 0.76, p = 0.015), *Bacteroides* (r = 0.67, p = 0.037), and *Fusobacterium* (r = 0.76, p = 0.015). GCDCA was significantly positively correlated with *Lactococcus* (r = 0.68, p = 0.035), *Pseudomonas* (r = 0.92, p = 0.0005), and *Clostridium* (r = 0.73, p = 0.020). GLCA was significantly positively correlated with *Lactococcus* (r=0.76, p=0.015), *Streptococcus* (r=0.81, p=0.007), *Escherichia* (r=0.83, p=0.005), and *Pseudomonas* (r=0.87, p=0.002).

12α-OH BAs, TDCA and GDCA, more effectively activated HSCs than other individual BAs

We then systematically screened individual BAs in HSC LX-2 cells, with the aim to determine the BA species that are most significantly contributing to the activation of HSC. These BAs included 12α-OH BAs (CA, TCA, GCA, DCA, TDCA, and GDCA), and non-12α-OH BAs (CDCA, TCDCA, GCDCA, LCA, GLCA, TLCA, UDCA, TUDCA, GUDCA) that were significantly increased in liver fibrosis patients and the three mouse models. The cells were treated with each BA at 25, 50, 75, and 100 μM for 24 h. Gene expression of HSC activation markers, including α-SMA, TGF-β, collagen I (COL I), and platelet-derived growth factor (PDGF) were measured using qRT-PCR after the treatments (Fig. S7). At higher BA concentrations (75 and 100 μM), most of the tested BAs upregulated the gene expression of α-SMA and TGF-β. However, only conjugated secondary 12α-OH BAs (i.e., TDCA and GDCA) effectively upregulated all of the HSC activation markers at both higher and lower (25 and 50 μM) concentrations, suggesting the conjugated secondary 12α-OH BAs are the predominant BA species that induce HSC activation.

We further investigated the incubation time of BAs on HSC activation, but removed UDCA and its conjugates from the test due to their protective effect on liver fibrosis. We also removed LCA, because of its low concentrations detected in plasma and liver. This secondary BA is mostly excreted into feces and only a small amount enters the enterohepatic circulation [30]. We treated LX-2 cells with the remaining BAs at 50 μM for 24, 48 and 72 h, and measured the gene expression of HSC activation markers, including α-SMA, TGF-β, and COL I using qRT-PCR (Fig. 4A). Overall, the highest expression levels of these markers were found at 24 hours, and decreased as the incubation time prolonged. Compared with non-12α-OH BAs, 12α-OH BAs induced higher fold increase.

We also compared the cell number of LX-2 cells after a 5-day incubation with 12α-OH and non-12α-OH BAs, at concentrations of 25, 50, 75 and 100 μM (Fig. S8). Again, TDCA and GDCA consistently increased cell number by 1.4-2 folds compared to vehicle control at all concentrations tested.

TDCA and GDCA showed the strongest effects in activating HSC and promoting HSC proliferation

Based on the findings on human and animal studies and our findings regarding HSC activation and proliferation by the individual BAs presented above, two BA combinations were setup to investigate the fibrogenic effects of altered BAs. We combined conjugated primary 12α-OH BAs (TCA and GCA), with equal amount of TCA (50 μM) and GCA (50 μM), termed as 12α-OH BA1. We also combined conjugated secondary 12α-OH BAs (TDCA and GDCA), with equal amount of TDCA (50 μM) and GDCA (50 μM), termed as 12α-OH BA2. The concentration (50 μM) was determined based on the BA concentrations found in the liver of liver fibrosis model mice. Immunofluorescent staining showed 12α-OH BA2 more significantly upregulated the protein expression of fibrotic markers α-SMA and TGF-β in LX-2 cells after a 48-h treatment than 12α-OH BA1 (Fig. 4B). These changes were further confirmed by western blotting (Fig. 4C). After 5 days of treatment, 12α-OH BA1 did not change the cell number of LX-2 cells, but 12α-OH BA2 significantly increased cell number on day 5 (Fig. 4D).

We further investigated the effects of 12α-OH BA1 or 12α-OH BA2 on liver fibrogenesis using an *in vitro* 3D model. The 3D culture system employed, contained human fetal hepatocyte L02 and LX-2 at a ratio of 100:1, to mimic cell-cell interactions in the liver. The cells were treated with 12α-OH BA1 and 12α-OH BA2 (each BA at 50 μM) for 5 days. Immunofluorescent staining showed that α-SMA, TGF-β, and COL I were highly expressed after 12α-OH BA2 treatment (Fig. 4E, 4F). We also observed that 12α-OH BA2 had a stronger effect on the expression of TGR5 than 12α-OH BA1 in the LX-2 HSC cell line (Fig. 4E, 4F).

Next, we studied liver fibrosis related signaling pathways that are downstream of TGR5. We treated LX-2 cells with 12α-OH BA1 and 12α-OH BA2 (same concentrations as above) for 24 hours, and analyzed protein expression of total and phosphorylated ERK1/2 and p38 MAPK using western blot analysis. The phosphorylation of ERK1/2 and p38 MAPK was not perceivably changed by 12α-OH BA1; however, 12α-OH BA2 treatment markedly increased both ERK1/2 and p-38 MAPK phosphorylation (Fig. 4G). No apparent difference in JNK activation (p-JNK) between 12α-OH BA1 treated and 12α-OH BA2 treated groups (Fig. 4G).

TDCA and GDCA were predicted to have the highest affinity to TGR5 among all BAs tested

Both FXR and TGR5 play important roles in liver fibrogenesis. Because FXR has extremely low expression in HSCs, it may not play a major role in HSC activation [31]. We hypothesized that 12α-OH BA2 have greater affinities to TGR5 than 12α-OH BA1 do, and therefore they were stronger LX-2 activators than 12α-OH BA1 were. To test this hypothesis, we performed a TGR5-BA affinity analysis using the Schrodinger Suite 2015-4. Results showed that BAs contacted Y89 in TGR5 from two sides (bottom and right), which explains how BAs, with a bendable shape, specifically interact with TGR5. As shown in Fig. S9A, five hydrogen bonds were formed between TDCA and TGR5, i.e., 3-hydroxyl to N93 and Y240, 12-hydroxyl to Y89, amide to S156, and sulfate to Q77, which explains why TDCA induced the strongest LX-2 activation among all the BAs tested. Figs. S8B and S8C further shows that compared with other BAs, TDCA and GDCA had lower binding free energy and lower median effective concentrations (EC50), and therefore had stronger binding affinity to TGR5.

Conjugated 12α-OH BAs promote liver fibrosis by activating TGR5/ERK1/2 and TGR5/p38 MAPK signaling pathways in HSCs

To further identify the signaling pathways involved in 12α-OH BA2-induced liver fibrosis, we treated LX-2 cells with 12α-OH BA1

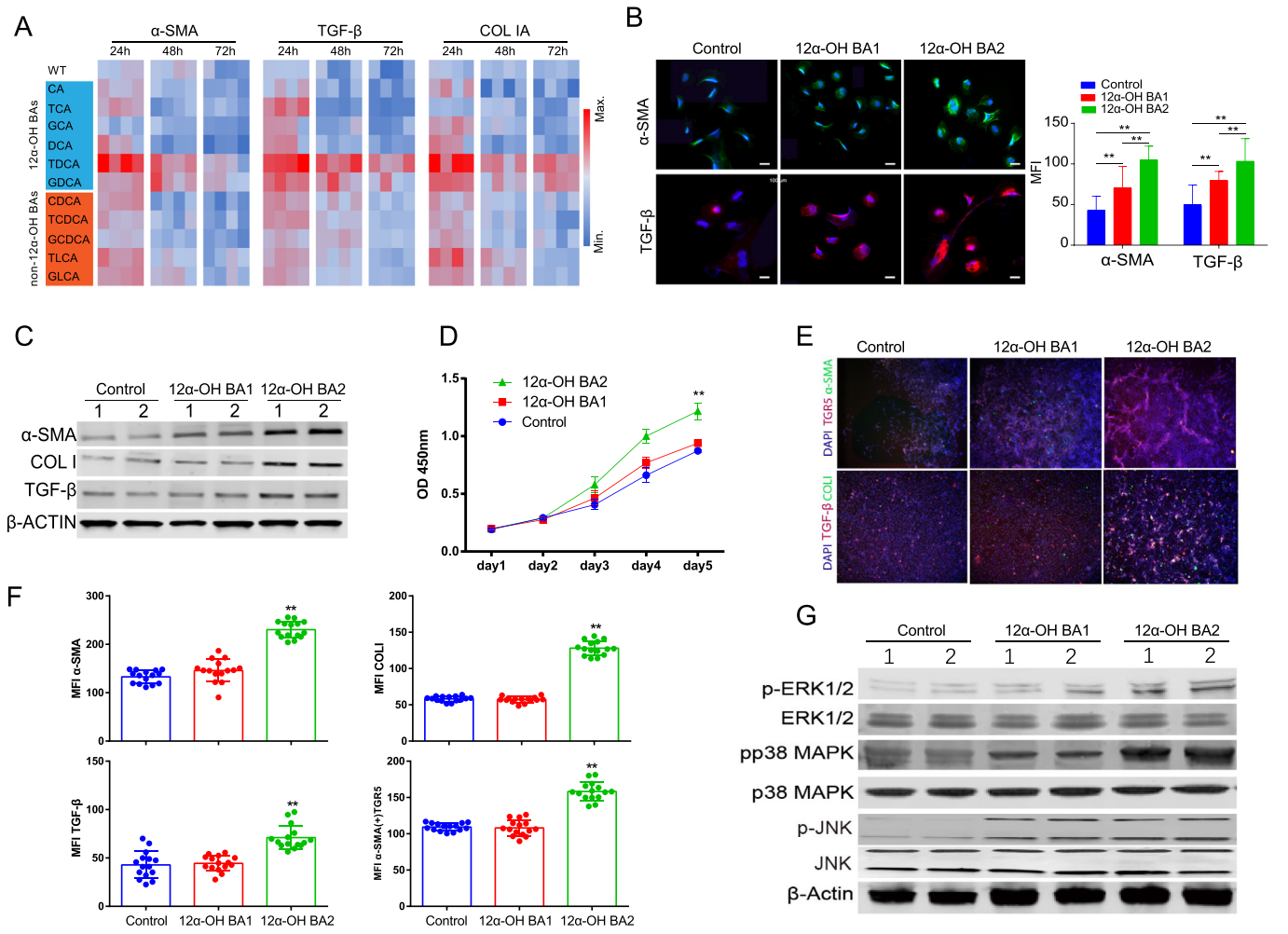

Fig. 4. Effects of conjugated primary 12α-OH BAs (12α-OH BA1) and conjugated secondary 12α-OH BAs (12α-OH BA2) on human hepatic stellate cells (HSC) LX-2. (A) Heatmap of gene expression level of α-SMA, TGF-β and COL I in LX-2 cells treated with different BAs (50 μM) for 24-72 hours. Relative gene expression was measured using quantitative real-time PCR (qRT-PCR), with GAPDH as housekeep gene. **(B)** Immunofluorescence staining for α-SMA and TGF-β in LX-2 cells treated with 50 μM 12α-OH BA1 or 12α-OH BA2 for 48 hours. The Mean Florescence Intensities (MFI) of five random microscopic views of each condition were quantified using Image J software. **(C)** Western-blot analysis of the protein expression level of α-SMA, TGF-β and COL I in LX-2 cells treated with 50 μM 12α-OH BA1 or 12α-OH BA2 for 48 hours. **(D)** Growth curves of LX-2 cells treated with vehicle control, 12α-OH BA1 or 12α-OH BA2 analyzed with a WST-8-based Cell Counting Kit. **(E)** Immunofluorescence staining of 3D cultured micro-tissues containing L02 and LX-2 (L02: LX-2 = 100:1) treated with 50 μM 12α-OH BA1, or 12α-OH BA2. **(F)** The Mean Florescence Intensities (MFI) of five random microscopic views of each condition were quantified using Image J software and presented for α-SMA, COL I, TGF-β, and TGR5 expression in α-SMA positive cells. **(G)** Phosphorylation of ERK1/2, p38MAPK, and JNK in LX-2 cells. Mean ± SD. * $p<0.05$ and ** $p<0.01$.

and 12α-OH BA2 for 5 min, 30 min, 2 h, 24 h, 48 h and 72 h, and analyzed phosphorylation of ERK1/2 and p38 MAPK using western blot analysis. Fig. 5A shows that for both treatments, the highest levels of ERK1/2 and p38/MAPK phosphorylation occurred at 5 min, and gradually decreased thereafter. The protein expression of the fibrotic marker α-SMA remained roughly equal from 5 min to 72 h within each type of treatment. Compared to 12α-OH BA1, 12α-OH BA2 resulted in stronger and longer-lasting phosphorylation of ERK1/2 and p38 MAPK, and higher levels of α-SMA protein expression at all times.

We postulated from the studies above that 12α-OH BA2 could promote HSCs proliferation and activation probably through TGR5 and its downstream signaling pathways such as ERK1/2 and p38 MAPK. To verify this hypothesis, we knocked down TGR5 expression in LX-2 cells using shRNA (Fig. S10A), and then analyzed LX-2 cell proliferation treated with 12α-OH BA1 and 12α-OH BA2. Knocking down TGR5 alone did not change cell number during the 5 days, but both 12α-OH BA1 and 12α-OH BA2 treatments significantly decreased cell number (Fig. S10B), through activating caspase 3-dependent apoptosis (Fig. S10C). Therefore, TGR5 is essential for the resistance to BA-induced apoptosis in HSCs. This finding is consistent with a previous report that TGR5 rendered anti-apoptosis ability in hepatocytes during liver injury [32].

To explore the 12α-OH BA2/TGR5 downstream signaling in LX2, first, we measured the intracellular cAMP level and we found that 12α-OH BA2 can boost cAMP significantly than 12α-OH BA1 (Fig. S11A). Next, we used a TGR5 antagonist 5β-cholanic acid [33,34] to investigate whether the liver fibrogenic promoting effects of 12α-OH BA2 are TGR5 dependent. We found that 5β-cholanic acid inhibited 12α-OH BA2-induced ERK1/2 and p38 MAPK phosphorylation, and α-SMA and COL-I upregulation (Fig. 5B and 5C). 5β-cholanic acid also significantly inhibited the pro-proliferative effect of 12α-OH BA2 on LX-2 cells (Fig. 5D).

To confirm that 12α-OH BA2 can activate HSC with significantly increased expression of α-SMA, COL I and TGR5 via activating ERK1/2 and p38 MAPK, we used the inhibitors of ERK1/2 (SCH772984), p38 MAPK (SB239063) or both of ERK1/2 inhibitor and p38 MAPK inhibitor, and JNK inhibitor (SP600125) to treat the BA activated HSCs. Fig. 5E shows that both SCH772984 and SB239063 inhibited the pro-proliferative effect of 12α-OH BA2, especially when the two inhibitors were combined; but SP600125 showed no effect on cell proliferation during 12α-OH BA2 treatment. Western blot (Fig. 5F) shows

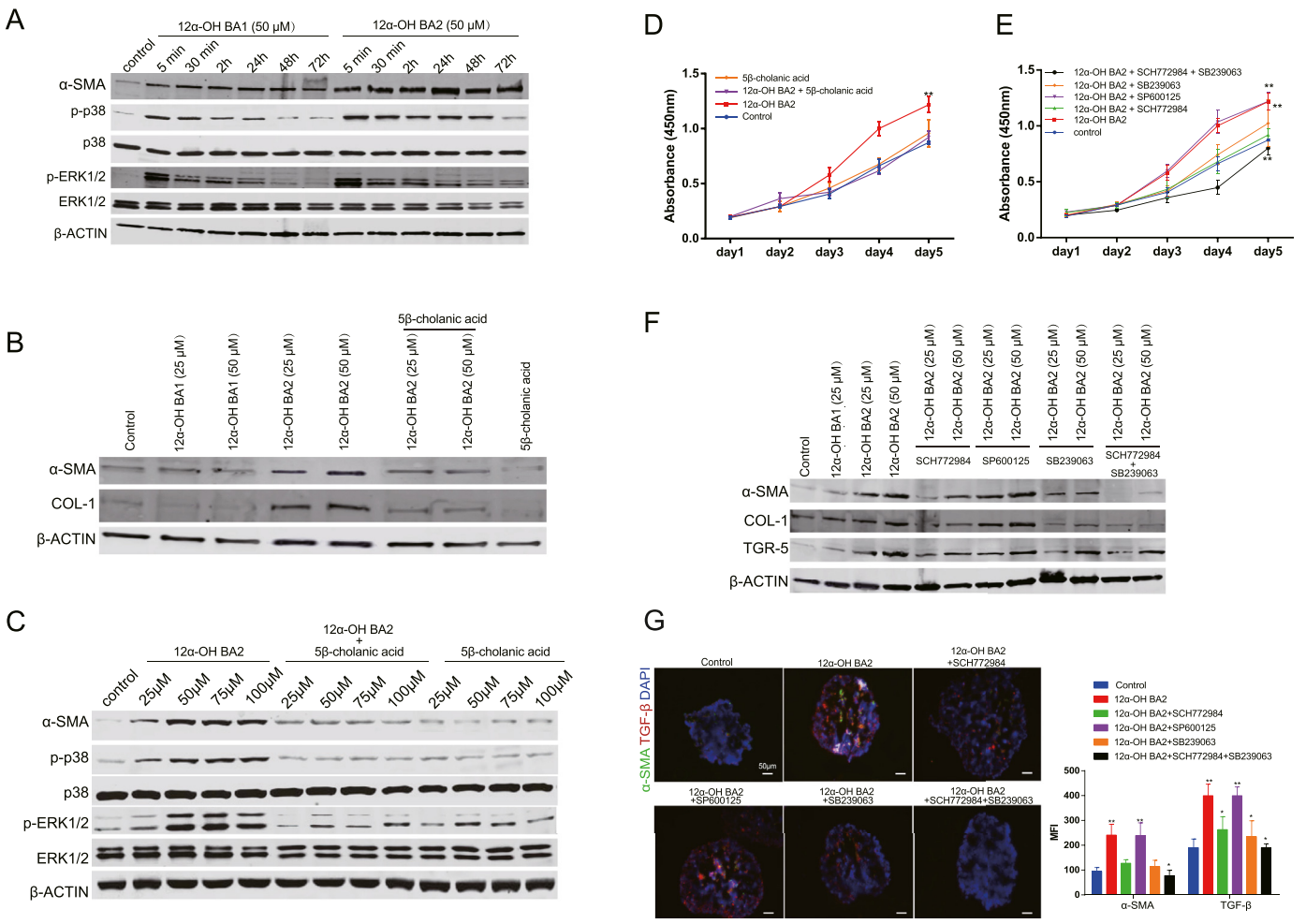

Fig. 5. TGR5 antagonist and inhibitors for ERK1/2 and p38MAPK abolished 12α-OH BA2-induced LX-2 activation. (A) Phosphorylation of ERK1/2 and p38MAPK detected by western blot in LX-2 cells treated with 12α-OH BA1 or 12α-OH BA2 (50 μM) for 5 min to 72 hours. **(B)** TGR5 antagonist 5β-cholanic acid (50 μM) inhibited 12α-OH BA2-induced overexpression of α-SMA and COL-1 proteins in LX-2 cells, as detected by western blot. **(C)** 5β-cholanic acid inhibited 12α-OH BA2-induced phosphorylation of ERK1/2 and p38/MAPK in LX-2 cells, as detected by western blot. **(D,E)** The pro-proliferative effect of 12α-OH BA2 in LX-2 cells was abolished by 5β-cholanic acid **(D)**, ERK1/2 inhibitor SCH772984 (100 μM), and p38 MAPK inhibitor SB239063 (50 μM) but not by JNK inhibitor SP600125 (50 μM) **(E)**. Cell numbers were quantified using a CCK-8 kit. **(F)** SCH772984 and SB239063, but not SP600125 inhibited 12α-OH BA2-induced overexpression of α-SMA, COL-I, and TGR5 in LX-2 cells, as detected using western blot. **(G)** SCH772984 and SB239063, but not SP600125 inhibited 12α-OH BA2-induced overexpression of α-SMA and TGF-β in the L02 and LX-2 composed 3D micro-tissues. The protein expression was detected using immunofluorescence staining. The data are presented as Mean ± SD. * $p<0.05$ and ** $p<0.01$. Treatments lasted for 48 hours if not stated otherwise.

that both SCH772984 and SB239063 inhibited 12α-OH BA2-induced upregulation of TGR5, α-SMA, and COL I protein expression, especially when the two inhibitors were combined; however, SP600125 had no effect on the expression of these proteins. This result was further confirmed in LX-2 cells that were co-cultured with L02 cells in the aforementioned 3D system (Fig. 5G). Therefore, we can conclude here that the fibrosis promoting effect of 12α-OH BA2 are TGR5/ERK1/2 and TGR5/p38MAPK dependent.

It is interesting that we found 12α-OH BA2 can increase the protein expression of TGR5 in a dose dependent manner (Fig. 5F). We wondered that whether 12α-OH BA2 can promote the transcription of Gpbar1, gene symbol for TGR5, and we further confirmed the promotion effect by using real-time PCR in LX2 cell. Meanwhile, to further explore the mechanism, different inhibitors targeting adenylyl cyclase (AC) (SQ22536), CREB (KG-501), p38MAPK (SGH772984) and p-ERK1/2 (SB239063) were used. We found that all inhibitors can significantly attenuate 12α-OH BA2 induced Gpbar1 transcription especially when AC and CREB activation were inhibited (Fig. S11B). We can conclude that the transcription of Gpbar1 can be triggered by 12α-OH BA2 through the downstream signaling pathways.

Expression of TGR5, p-p38 MAPK, and p-ERK1/2 was significantly increased in STZ-HFD-treated mice and liver fibrosis patients

As shown in Fig. 2D and Fig. 6A, trichrome staining showed significantly increased fibrotic area in the liver in STZ-HFD treated mice. Immunohistochemical staining showed that significantly increased protein expression of α-SMA, TGF-β, COL I and PDGF in the liver (Fig. 6A). Immunofluorescence staining also showed markedly elevated protein expression of TGR5, TGF-β, and phosphorylation of ERK1/2 and p38 MAPK in the liver of the STZ-HFD-treated mice (Fig. 6B). In addition, immunofluorescence staining of normal human liver tissues (n = 20) and patients with liver fibrosis (n = 20) further confirmed that the activity and expression of TGR5, p-p38 MAPK and p-ERK1/2 were significantly increased in liver fibrosis patients (Fig. 6C).

TDCA and GDCA promoted liver fibrosis in CCl_4-induced liver fibrosis C57BL/6J mice

Results obtained from *in vitro* studies indicated that TDCA and GDCA effectively activated HSCs and promote liver fibrosis. We thus

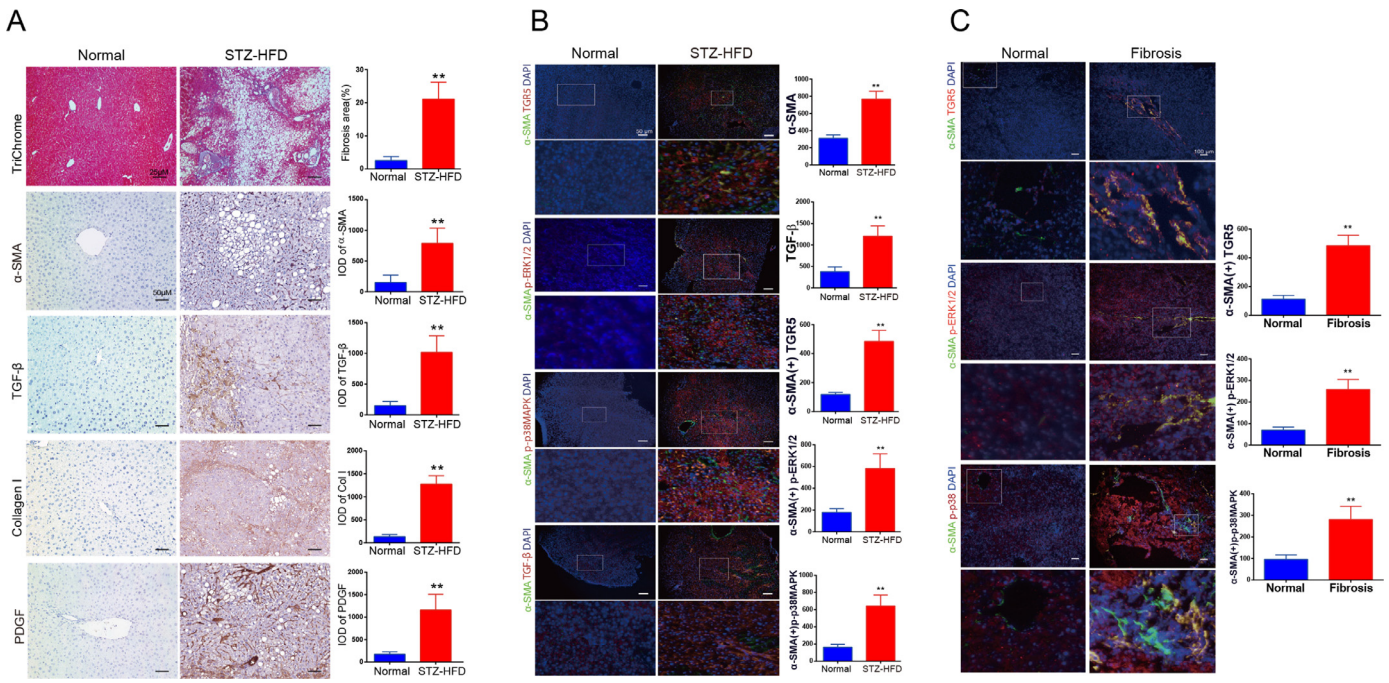

Fig. 6. Expression of TGR5, p-p38 MAPK and p-ERK1/2 was significantly increased in STZ-HFD-treated mice and liver fibrosis patients. (A) Liver fibrosis detected by Masson Trichrome staining, and protein expression of α-SMA, TGF-β, COL-1, and PDGF in the mouse liver detected by immunohistochemistry staining. **(B)** Protein expression of TGR5, TGF-β, and phosphorylation of p-ERK1/2 and p-p38 MAPK, as detected by immunofluorescence staining. The MFI of 15 random microscopic views of each condition were quantified using the Image J software. **(C)** Immunofluorescence staining for ERK1/2 and p38MAPK phosphorylation and TGR5 expression in α-SMA-positive cells in the liver of patients with liver fibrosis and controls. The MFI of 15 random visions of each sample were quantified using Image J software. Mean±SD. [a] $p<0.05$ compared to normal, [b] $p<0.05$ compared to STZ-HFD. * $p<0.05$ and ** $p<0.01$ vs. normal. Mouse study, n=8 per group; human study, n=15 per group.

used the CCl_4-induced liver fibrosis mouse model to investigate the role of TDCA and GDCA in liver fibrogenesis. The mice were treated with CCl_4, or TDCA + GDCA, or TDCA+GDCA +CCl_4, or treated with corn oil as control. After 5-week treatment, liver to body weight ratio and serum levels of ALT and AST in the serum and liver were significantly increased in CCl_4 model mice, TDCA + GDCA treated mice and further increased in TDCA + GDCA + CCl_4 treated mice (Fig. 7A).

Immunohistochemical staining showed that Tgr5 expression was the strongest in α-SMA positive cells in TDCA + GDCA + CCl_4 treated mice. The activation of ERK1/2 and p38 MAPK was increased significantly in CCl_4 and TDCA+GDCA treated mice and further increased in TDCA+GDCA + CCl_4 treated mice (Fig. 7B). Immunohistochemical staining also showed that TDCA and GDCA treatment significantly increased protein expression of α-SMA, TGF-β, and COL I in the liver of the treated mice (Fig. 7C). Masson trichrome staining showed significant increased collagen level in TDCA and GDCA, or CCl_4 treated mice. We found even more significant increase of collagen level in the liver of TDCA+GDCA + CCl_4 treated mice (Fig. 7C).

Depletion of Tgr5 in HSCs significantly decreased liver fibrosis

Since results obtained from *in vivo* and *in vitro* studies indicated that TGR5 was essential in HSCs activation and NASH-associated liver fibrosis, we therefore investigated the role of TGR5 in liver fibrogenesis. We isolated HSCs from CAS9 KI mice ($HSCs^{CAS9\ KI}$) and then treated with Tgr5 sgRNA adeno-associated virus (AAV) ($HSCs^{CAS9\ KI+Tgr5sgRNA}$). We found that the expression of Tgr5 in HSCs can be effectively depleted due to the expression of CAS9 (Fig. S12). We then treated the $HSCs^{CAS9\ KI}$ and $HSCs^{CAS9\ KI+Tgr5sgRNA}$ with 12α-OH BA2 and observed significantly decreased proliferation as well as decreased expression of α-SMA, COL I, TGF-β in $HSCs^{CAS9\ KI+Tgr5sgRNA}$ compared to $HSCs^{CAS9\ KI}$ (Fig. 8A, B).

We further used the CCl_4-induced liver fibrosis mice model to investigate the role of HSCs-Tgr5 signaling in liver fibrosis. The CAS9 KI mice were treated with CCl_4 (CAS9 KI+ CCl_4), or treated with AAV virus containing Gfap-Cre-U6-Tgr5 sgRNA cassette (CAS9 KI+ CCl_4+Tgr5 sgRNA) via intrasplenic injection plus CCl_4, or treated with corn oil as control. Masson trichrome and α-SMA staining showed significant decreased collagen level and α-SMA positive cells (activated HSCs) in the liver of CAS9 KI+ CCl_4+Tgr5 sgRNA mice (Fig. 8C) after a 5-week treatment. Tgr5 expression in α-SMA positive cells was strongest in CAS9 KI+ CCl_4 mice, and the expression of Tgr5 in α-SMA positive cells was almost totally depleted due to the specific expression of CAS9 induced by Gfap promoter (Fig. 8D and S8). The activation of ERK1/2 and p38 MAPK signaling was decreased significantly in CAS9 KI+ CCl_4+Tgr5 sgRNA group (Fig. 8D).

Discussion

In 1996, CA, CDCA, LCA, and UDCA were shown to induce protein kinase C (PKC)-dependent MAPK phosphorylation in rat HSCs at physiologically relevant concentrations [35]. In 2005, CA, GCDCA, and TUDCA were shown to induce rat HSC proliferation via EGFR [36]. In 2010, reports also showed that TDCA treatment could stimulate cell proliferation depends on upregulation of NOX5-S through activation of the TGR5 [37]. In 2018, secondary unconjugated BAs such as DCA was reported to be able to induce the activation of human HSCs [38]. A recent study on the investigation of primary BAs, CDCA (non 12α-OH BAs) and CA (12α-OH BAs) showed that both CDCA and CA can promote the activation and proliferation of HSCs [39,40]. In reference to these studies, our study made the following progress: (1) We systematically screened multiple BA species, including the 12α-OH BAs (CA, DCA, and their taurine- and glycine-conjugated derivatives), and non-12α-OH (CDCA, LCA, and UDCA, and their taurine- and glycine-conjugated derivatives). All BAs were tested for their HSC activating ability based on their regulatory effects on gene expression of HSC activation markers. We found that conjugated secondary 12α-OH BAs, TDCA and GDCA, most effectively upregulated all the markers

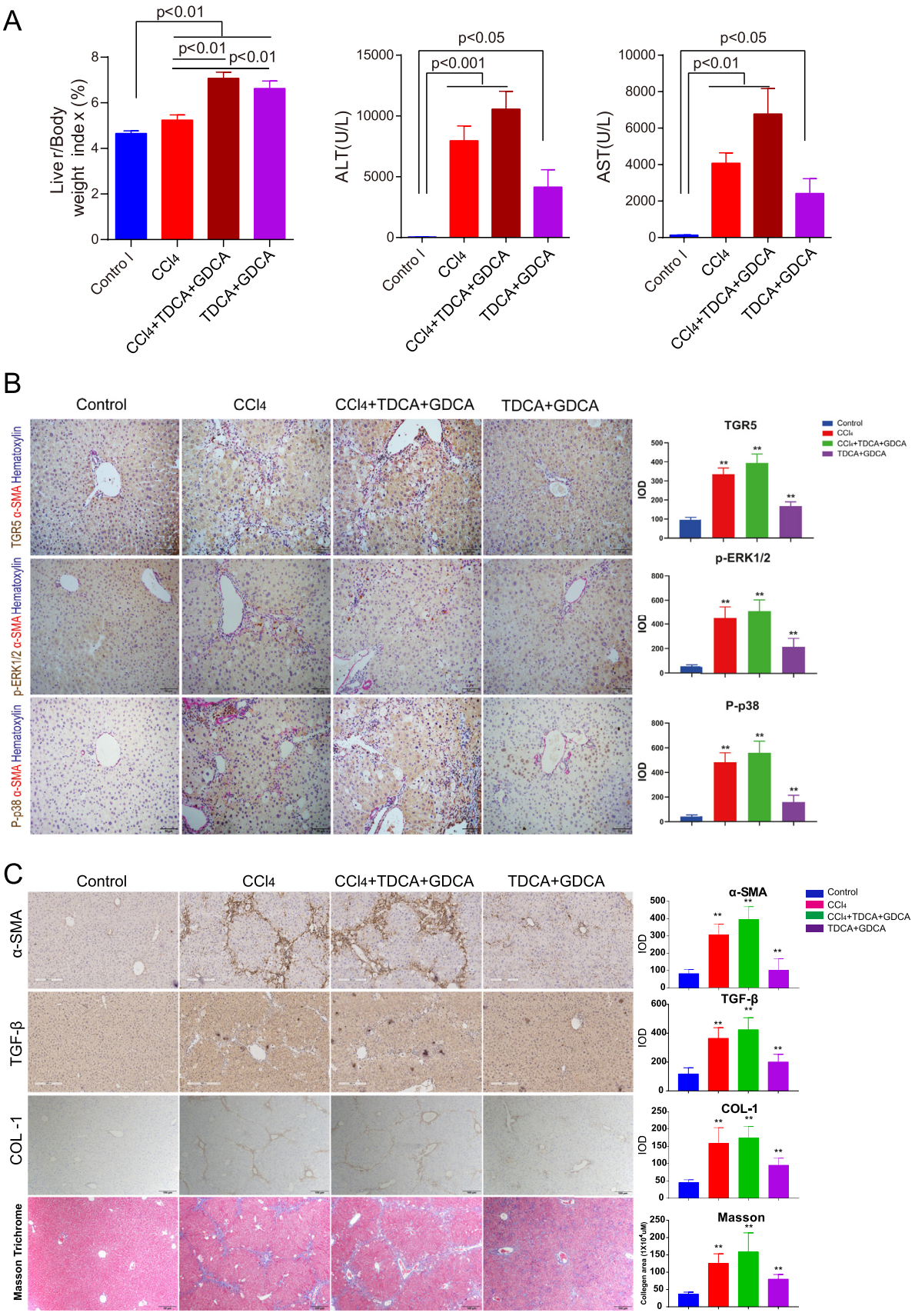

Fig. 7. TDCA and GDCA significantly promote liver fibrosis in CCl_4-induced liver fibrosis C57BL/6J model mice. (A) Bar plots of liver to body weight ratio, serum levels of ALT and AST. **(B)** Tgr5 expression, activation of ERK1/2 and p38MAPK in α-SMA positive cells in mice liver as determined by IHC staining ($\times$ 200). **(C)** Protein expression of α-SMA, TGF-β, and COL-1 in the liver detected by immunohistochemistry staining. The collagen level in mice liver as determined by Masson Trichrome staining ($\times$ 100).

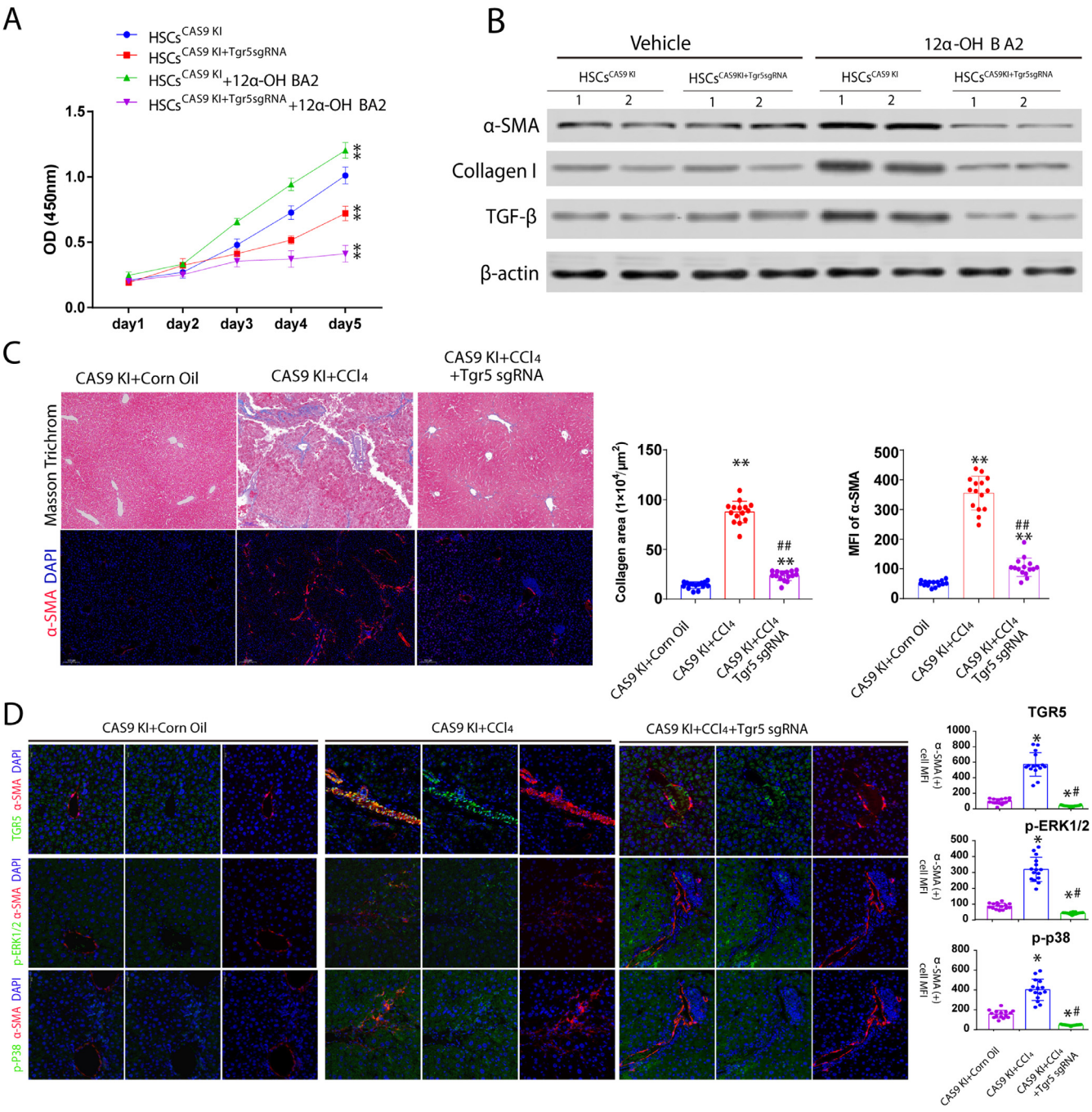

Fig. 8. Depletion of Tgr5 in HSCs significantly decreased liver fibrosis in a CCl_4-induced liver fibrosis model mouse. (A) Proliferation of primary HSCs cells as evaluated using a CCK-8 kit. **(B)** The protein expression of α-SMA, Collagen I and Tgf-β in $HSCs^{CAS9\ KI}$ and $HSCs^{CAS9\ KI+Tgr5sgRNA}$ treated with 50 μM 12α-OH BA2 and vehicle control, a, $p<0.01$, two-way ANOVA. **(C)** The collagen level and α-SMA in mice liver as determined by Masson Trichrome and IF staining ($\times$ 100). **(D)** Tgr5 expression, activation of p-Erk1/2 and p-p38Mapk in α-SMA positive cells in mice liver as determined by IF staining ($\times$ 300). *, compared to CAS9 KI Corn Oil, by Student's t-test; #, compared to CAS9 KI+ CCl_4, by Student's t-test.

tested at a concentration as low as 25 μM. This finding was further confirmed at multiple time points, and corroborated by cell number increases after a 5-day incubation; (2) Our computational modeling predicted binding affinity data, and confirmed the role of TDCA and GDCA in liver fibrogenesis using a CCl_4-induced liver fibrosis C57BL/6J mouse model. We demonstrated the critical role of TGR5 in HSC activation using 5β-cholanic acid (a TGR5 inhibitor), and confirmed the finding using a CCl_4-induced liver fibrosis Rosa26-LSL-Cas9 knockin mouse model with depleted Tgr5 in HSCs. Recent publications suggest that TGR5 is likely located upstream of previously reported signaling molecules involved in HSC activation, such as PKC [41], EGFR [42], and NOX5-S [37]. As a membrane receptor, TGR5 activation does not require cellular uptake of BAs, which is in line with the observation that BAs did not enter HSCs [36]; (3) This study adopted a systems approach, and examined the combined effects of multiple BAs, for longer periods of time, and also used a 3D co-culture system to more closely mimic the *in vivo* condition. These differences in experimental condition may also explain why we found BAs increased the expression of COL I and TGF-β in HSCs, differing from a previous report [36].

Our results showed that 12α-OH BAs, in particular, TDCA and GDCA, more effectively activated HSCs than the rest of BAs. In line

with our results, secondary BAs (DCA and LCA) were found to more effectively activate TGR5 than primary BAs (CA and CDCA) [43]. Therefore, the gut microbe-dependent production of DCA, and its enterohepatic circulation and conjugation in the liver, are of profound significance in liver fibrogenesis. We previously reported that STZ-HFD treatment in mice induced significant alteration of gut microbiota [26], and substantially increased levels of hydrophobic BAs, including DCA, TDCA, TLCA, TCA, and TCDCA, in liver and plasma [25]. In turn, dysregulated intestinal BAs may cause increased absorption of bacterial lipopolysaccharides, and thereby promote systemic inflammation and further stimulate HSC proliferation [44]. In addition to TGR5-mediated signal transduction, DCA also promoted obesity-associated HCC development in mice via inducing a senescence-associated secretory phenotype in HSCs [45], and TLCA impaired BA flow in rat liver, leading to cholestasis [46]. The intracellular nuclear receptor FXR and the transmembrane G protein-coupled receptor TGR5 respond to BAs by activating transcriptional networks and/or signaling cascades. FXR is the primary hepatic BA sensor [47] and studied most extensively for its regulation of numerous genes involved in BA homeostasis [48,49]. In addition to its role in regulating BA synthesis, excretion, and transport [48,49], emerging evidence showed that FXR might also play a pivotal role in liver fibrosis via regulating HSCs activity [31,50]. FXR has been reported to be expressed in HSCs and exposure of HSCs to FXR ligands down-regulated α1(I) collagen mRNA expression and collagen synthesis [50]. TGR5 activation alone has been reported to induce the expression of interleukin 1β (IL-1β) and tumor necrosis factor-a (TNF-α) in murine macrophage cell line RAW264.7 or murine Kupffer cells, which was correlated with the suppression of cholesterol 7a-hydroxylase (Cyp7a1) expression in murine hepatocytes [51]. TGR5 is also expressed in HSCs when they are activated [12], and without TGR5, HSCs showed no significant differentiation after BA treatment [13]. These results suggest that the induction of FXR and TGR5 by BAs may differ between 12α-OH BAs and non-12α-OH BAs, and the activation of HSC by BAs may depend on the balance of their effects on FXR and TGR5.

Our study confirmed that TDCA and GDCA administration promoted liver fibrosis and that depletion of Tgr5 in HSCs in mice mitigated liver fibrosis in a CCl_4-induced liver fibrosis model mouse. The proliferation and activation of HSCs were significantly reduced and the activation of ERK1/2 and p38 MAPK signaling was also decreased significantly due to Tgr5 depletion. The inhibition of BA-induced HSC activation by antagonizing TGR5 signal transduction may lead to effective prevention or remission of liver fibrosis.

In summary, this study demonstrated that liver fibrosis was associated with elevated BAs (especially conjugated 12α-OH BAs) in the circulation of both humans and mice. Pathologically high levels of 12α-OH BAs induced HSC activation, and this effect was more pronounced with conjugated secondary 12α-OH BAs (i.e., TDCA and GDCA). TGR5, ERK1/2, and p38 MAPK were essential signaling mediators of the BA-induced HSC activation. Reduction of p38 MAPK and ERK 1/2 phosphorylation or inhibition of TGR5 expression can significantly reduce proliferation and activation of HSC. This study suggests that antagonizing TGR5 or inhibiting ERK1/2 and p38 MAPK signaling may effectively prevent or reverse liver fibrosis.

Author contributions

W.J. was principal investigator of this study and designed the study. P.L., X.G., H.B., B.C.S. organized the patient recruitment and provided biospecimens for this study. B.C.S. led the animal experiments on CCl_4-induced liver fibrosis Rosa26-LSL-Cas9 knock in mouse model and provided biospecimens. G.X.X. drafted the manuscript. G.X.X., R.Q.J., C.R., and W.J. critically revised the manuscript. G. X.X., R.Q.J., X.N.W., A.H.Z., F.J.H., Z.P.L., J.N.Q., X.J.Z. and X.L.Z. performed experiments on animal and cells, collected samples, analyze samples and the data. Y.R.W. and S.W.Z. performed the bile acid-TGR5 binding affinity analysis. All authors edited the manuscript and approved the final manuscript.

Declaration of Competing Interests

The authors declare no competing interests.

Acknowledgments

This study was financially supported by the National Institutes of Health/National Cancer Institute Grant 1U01CA188387-01A1, the National Key Research and Development Program of China (2017YFC0906800); the State Key Program of National Natural Science Foundation (81430062); the National Natural Science Foundation of China (81974073, 81774196), China Postdoctoral Science Foundation funded project, China (2016T90381), and E-institutes of Shanghai Municipal Education Commission, China (E03008). The Funders did not have any role in study design, data collection, data analyses, interpretation, or writing of this manuscript.

Data availability statement

All the data supporting the findings of this study are available within the article and its Supplementary Information files or from the corresponding author upon reasonable request.

Supplementary materials

Supplementary material associated with this article can be found, in the online version, at doi:10.1016/j.ebiom.2021.103290.

References

[1] Shneider BL, Gonzalez-Peralta R, Roberts EA. Controversies in the management of pediatric liver disease: Hepatitis B, C and NAFLD: summary of a single topic conference. Hepatology 2006;44(5):1344–54.
[2] Calzadilla Bertot L, Adams LA. The natural course of non-alcoholic fatty liver disease. Int J Mol Sci 2016;17(5):774.
[3] Bugianesi E, Leone N, Vanni E, et al. Expanding the natural history of nonalcoholic steatohepatitis: from cryptogenic cirrhosis to hepatocellular carcinoma. Gastroenterology 2002;123(1):134–40.
[4] McPherson S, Hardy T, Henderson E, Burt AD, Day CP, Anstee QM. Evidence of NAFLD progression from steatosis to fibrosing-steatohepatitis using paired biopsies: Implications for prognosis and clinical management. J Hepatol 2015;62(5):1148–55.
[5] Chang TT, Liaw YF, Wu SS, et al. Long-term entecavir therapy results in the reversal of fibrosis/cirrhosis and continued histological improvement in patients with chronic hepatitis B. Hepatology 2010;52(3):886–93.
[6] George SL, Bacon BR, Brunt EM, Mihindukulasuriya KL, Hoffmann J, Di Bisceglie AM. Clinical, virologic, histologic, and biochemical outcomes after successful HCV therapy: a 5-year follow-up of 150 patients. Hepatology 2009;49(3):729–38.
[7] Beyoglu D, Idle JR. The metabolomic window into hepatobiliary disease. J Hepatol 2013;59(4):842–58.
[8] Chiang JY. Bile acid metabolism and signaling. Comprehensive Physiol 2013;3(3):1191–212.
[9] Jia W, Xie G, Jia W. Bile acid-microbiota crosstalk in gastrointestinal inflammation and carcinogenesis. Nat Rev Gastroenterol Hepatol 2018;15(2):111–28.
[10] Thomas C, Pellicciari R, Pruzanski M, Auwerx J, Schoonjans K. Targeting bile-acid signalling for metabolic diseases. Nat Rev Drug Discov 2008;7(8):678–93.
[11] Sayin SI, Wahlström A, Felin J, et al. Gut microbiota regulates bile acid metabolism by reducing the levels of tauro-beta-muricholic acid, a naturally occurring FXR antagonist. Cell Metab 2013;17(2):225–35.
[12] Keitel V, Donner M, Winandy S, Kubitz R, Haussinger D. Expression and function of the bile acid receptor TGR5 in Kupffer cells. Biochem Biophys Res Commun 2008;372(1):78–84.
[13] Sawitza I, Kordes C, Gotze S, Herebian D, Haussinger D. Bile acids induce hepatic differentiation of mesenchymal stem cells. Sci Rep 2015;5:13320.
[14] Pandak WM, Kakiyama G. The acidic pathway of bile acid synthesis: not just an alternative pathway. Liver Res 2019;3(2):88–98.
[15] Haeusler RA, Pratt-Hyatt M, Welch CL, Klaassen CD, Accili D. Impaired generation of 12-hydroxylated bile acids links hepatic insulin signaling with dyslipidemia. Cell Metab 2012;15(1):65–74.

[16] Brufau G, Stellaard F, Prado K, et al. Improved glycemic control with colesevelam treatment in patients with type 2 diabetes is not directly associated with changes in bile acid metabolism. Hepatology 2010;52(4):1455–64.
[17] Puri P, Daita K, Joyce A, et al. The presence and severity of nonalcoholic steatohepatitis is associated with specific changes in circulating bile acids. Hepatology 2018;67(2):534–48.
[18] Wei M, Huang F, Zhao L, et al. A dysregulated bile acid-gut microbiota axis contributes to obesity susceptibility. EBioMedicine 2020;55:102766.
[19] Huang F, Zheng X, Ma X, et al. Theabrownin from Pu-erh tea attenuates hypercholesterolemia via modulation of gut microbiota and bile acid metabolism. Nat Commun 2019;10(1):4971.
[20] Tan Z, Qian X, Jiang R, et al. IL-17A plays a critical role in the pathogenesis of liver fibrosis through hepatic stellate cell activation. J Immunol (Baltimore, Md: 1950) 2013;191(4):1835–44.
[21] Tang J, Zhuo H, Zhang X, et al. A novel biomarker Linc00974 interacting with KRT19 promotes proliferation and metastasis in hepatocellular carcinoma. Cell Death Dis 2014;5:e1549.
[22] Jiang R, Tan Z, Deng L, et al. Interleukin-22 promotes human hepatocellular carcinoma by activation of STAT3. Hepatology 2011;54(3):900–9.
[23] Carpenter B, Nehme R, Warne T, Leslie AG, Tate CG. Erratum: structure of the adenosine A2A receptor bound to an engineered G protein. Nature 2016;538 (7626):542.
[24] Xie G, Zhong W, Li H, et al. Alteration of bile acid metabolism in the rat induced by chronic ethanol consumption. FASEB J 2013;27(9):3583–93.
[25] Xie G, Wang X, Huang F, et al. Dysregulated hepatic bile acids collaboratively promote liver carcinogenesis. Int J Cancer 2016;139(8):1764–75.
[26] Xie G, Wang X, Liu P, et al. Distinctly altered gut microbiota in the progression of liver disease. Oncotarget 2016;7(15):19355–66.
[27] Gomez-Hurtado I, Santacruz A, Peiro G, et al. Gut microbiota dysbiosis is associated with inflammation and bacterial translocation in mice with CCl4-induced fibrosis. PLoS One 2011;6(7):e23037.
[28] Zheng X, Huang F, Zhao A, et al. Bile acid is a significant host factor shaping the gut microbiome of diet-induced obese mice. BMC Biol 2017;15(1):120.
[29] Wang X, Xia J, Jiang C. Role of gut microbiota in the development of non-alcoholic fatty liver disease. Liver Res 2019;3(1):25–30.
[30] Chiang JY. Bile acids: regulation of synthesis. J Lipid Res 2009;50(10):1955–66.
[31] Fickert P, Fuchsbichler A, Moustafa T, et al. Farnesoid X receptor critically determines the fibrotic response in mice but is expressed to a low extent in human hepatic stellate cells and periductal myofibroblasts. Am J Pathol 2009;175 (6):2392–405.
[32] Keitel V, Reich M, Sommerfeld A, Kluge S, Kubitz R, Häussinger D. Role of the bile acid receptor TGR5 (Gpbar-1) in liver damage and regeneration. Eur J Med Res 2014;19(Suppl 1) S21-S.
[33] Renga B, Bucci M, Cipriani S, et al. Cystathionine gamma-lyase, a H2S-generating enzyme, is a GPBAR1-regulated gene and contributes to vasodilation caused by secondary bile acids. Am J Physiol Heart Circulatory Physiol 2015;309(1):H114–26.
[34] Sepe V, Renga B, Festa C, et al. Investigation on bile acid receptor regulators. Discovery of cholanoic acid derivatives with dual G-protein coupled bile acid receptor 1 (GPBAR1) antagonistic and farnesoid X receptor (FXR) modulatory activity. Steroids 2016;105:59–67.
[35] Brady LM, Beno DW, Davis BH. Bile acid stimulation of early growth response gene and mitogen-activated protein kinase is protein kinase C-dependent. Biochem J 1996;316(Pt 3):765–9.
[36] Svegliati-Baroni G, Ridolfi F, Hannivoort R, et al. Bile acids induce hepatic stellate cell proliferation via activation of the epidermal growth factor receptor. Gastroenterology 2005;128(4):1042–55.
[37] Hong J, Behar J, Wands J, et al. Role of a novel bile acid receptor TGR5 in the development of oesophageal adenocarcinoma. Gut 2010;59(2):170–80.
[38] Saga K, Iwashita Y, Hidano S, et al. Secondary unconjugated bile acids induce hepatic stellate cell activation. Int J Mol Sci 2018;19(10).
[39] Yarde SS, Cheng X. Primary and secondary bile acids activate hepatic stellate cells. FASEB J 2020;34(S1):1.
[40] Zhou J, Huang N, Guo Y, et al. Combined obeticholic acid and apoptosis inhibitor treatment alleviates liver fibrosis. Acta Pharm Sinica B 2019;9(3):526–36.
[41] Lieu T, Jayaweera G, Zhao P, et al. The bile acid receptor TGR5 activates the TRPA1 channel to induce itch in mice. Gastroenterology 2014;147(6):1417–28.
[42] Nagathihalli NS, Beesetty Y, Lee W, et al. Novel mechanistic insights into ectodomain shedding of EGFR Ligands Amphiregulin and TGF-alpha: impact on gastrointestinal cancers driven by secondary bile acids. Cancer Res 2014;74(7):2062–72.
[43] Duboc H, Tache Y, Hofmann AF. The bile acid TGR5 membrane receptor: from basic research to clinical application. Digestive and liver disease: official journal of the Italian society of gastroenterology and the Italian association for the study of the. Liver 2014;46(4):302–12.
[44] Toda K, Kumagai N, Tsuchimoto K, et al. Induction of hepatic stellate cell proliferation by LPS-stimulated peripheral blood mononuclear cells from patients with liver cirrhosis. J Gastroenterol 2000;35(3):214–20.
[45] Allen K, Jaeschke H, Copple BL. Bile acids induce inflammatory genes in hepatocytes: a novel mechanism of inflammation during obstructive cholestasis. Am J Pathol 2011;178(1):175–86.
[46] Beuers U, Bilzer M, Chittattu A, et al. Tauroursodeoxycholic acid inserts the apical conjugate export pump, Mrp2, into canalicular membranes and stimulates organic anion secretion by protein kinase C-dependent mechanisms in cholestatic rat liver. Hepatology 2001;33(5):1206–16.
[47] Makishima M, Okamoto AY, Repa JJ, et al. Identification of a nuclear receptor for bile acids. Science 1999;284(5418):1362–5.
[48] Chiang JY. Bile acid regulation of gene expression: roles of nuclear hormone receptors. Endocr Rev 2002;23(4):443–63.
[49] Chiang JY. Regulation of bile acid synthesis: pathways, nuclear receptors, and mechanisms. J Hepatol 2004;40(3):539–51.
[50] Fiorucci S, Antonelli E, Rizzo G, et al. The nuclear receptor SHP mediates inhibition of hepatic stellate cells by FXR and protects against liver fibrosis. Gastroenterology 2004;127(5):1497–512.
[51] Lou G, Ma X, Fu X, et al. GPBAR1/TGR5 Mediates Bile Acid-Induced Cytokine Expression in Murine Kupffer Cells. PLoS One 2014;9(4):e93567.